Pure Appl. Geophys. 171 (2014), 2185–2198

DOI 10.1007/s00024-014-0780-4

Pure and Applied Geophysics

SH Wave Number Green's Function for a Layered, Elastic Half-Space. Part I: Theory and Dynamic Canyon Response by the Discrete Wave Number Boundary Element Method

Doriam Restrepo,[1] Juan David Gómez,[1] and Juan Diego Jaramillo[1]

Abstract—We present a closed-form frequency-wave number ($\omega - k$) Green's function for a layered, elastic half-space under SH wave propagation. It is shown that for every ($\omega - k$) pair, the fundamental solution exhibits two distinctive features: (1) the original layered system can be reduced to a system composed by the uppermost superficial layer over an equivalent half-space; (2) the fundamental solution can be partitioned into three different fundamental solutions, each one carrying out a different physical interpretation, i.e., an equivalent half-space, source image impact, and dispersive wave effect, respectively. Such an interpretation allows the proper use of analytical and numerical integration schemes, and ensures the correct assessment of Cauchy principal value integrals. Our method is based upon a stiffness-matrix scheme, and as a first approach we assume that observation points and the impulsive SH line-source are spatially located within the uppermost superficial layer. We use a discrete wave number boundary element strategy to test the benefits of our fundamental solution. We benchmark our results against reported solutions for an infinitely long circular canyon subjected to oblique incident SH waves within a homogeneous half-space. Our results show an almost exact agreement with previous studies. We further shed light on the impact of horizontal strata by examining the dynamic response of the circular canyon to oblique incident SH waves under different layered half-space configurations and incident angles. Our results show that modifications in the layering structure manifest by larger peak ground responses, and stronger spatial variability due to interactions of the canyon geometry with trapped Love waves in combination with impedance contrast effects.

Key words: Layered half-space, Green's functions, Boundary elements, SH wave, Dynamic canyon response.

1. Introduction

Green's functions have been extensively recognized as a subject of fundamental importance in areas such as soil dynamics, acoustics, wave propagation problems in elasticity, and electromagnetism. Their most noticeable feature stems from the fact that Green's functions provide exact solutions of systems to transient point sources, therefore, only a conventional convolution scheme is required to obtain the system response to sources of more complex spatial distribution, and arbitrary variation in time.

A generally prevalent mathematical approach for computing Green's functions in geophysical research is the Fourier–Hankel transform. In this approach, initial partial differential equations are transformed into first-order differential equations expressed in the frequency-wave number azimutal domain, while keeping the vertical spatial coordinate unmodified. The formalism to study transformed representations of displacements and stresses of the Earth's crust or upper mantle as an elastic, layered half-space was initially introduced by Thomson (1950) and Haskell (1953). Since these pioneering studies, a large and growing body of variants have been presented, most of which have been focused on removing former numerical instabilities, and improving the computational efficiency of the Thomson–Haskell propagator matrix (e.g., Knopoff 1964; Dunkin 1965; Gilbert and Backus 1966; Kennett and Kerry 1979; Kennett 1983; Chin *et al.* 1984; Schmidt and Tango 1986; Wang and Rokhlin 2002; Chapman 2003). A particularly important method derived from the Thomson–Haskell scheme is the stiffness matrix approach (Kausel and Roësset 1981). In this method, local forces applied at the interfaces of the layers are related to displacements at the same locations through layer stiffness matrices. A global impedance matrix is assembled in the same way as in conventional structural analysis studies. Although the stiffness matrix approach is just a simple re-arrangement of elements

[1] Civil Engineering, Universidad EAFIT, Carrera 49 N 7 Sur-50, Medellín, Colombia. E-mail: drestre6@eafit.edu.co

in the original Thomson–Haskell propagator matrix, important advantages such as stability for thick layers, robustness at high frequencies, and reductions of the computational effort up to 8× can be achieved (Kausel 2006).

To date, the literature of Green's functions in layered half-spaces based upon some variation of the Thomson–Haskell propagator matrix is rather extensive (e.g., Fuchs and Müller 1971; Apsel and Luco 1983; Luco and Apsel 1983; Chen 1990; Hisada 1994, 1995; Wang 1999). These fundamental solutions, however, have been limited mostly to compute seismogram synthesis radiated from point and dipole sources (e.g., Bouchon 1981). Moreover, it appears as though they were never intended to be used in problems with potential engineering application such as the diffraction of plane waves by irregular scatterers. Unfortunately, the transition from studying synthetic realizations to studying the elastodynamic response of irregular bodies within layered media by means of Thomson–Haskell-like Green's functions is not simple. In general, the algebra and computer codes demanded are not trivial (Chapman 2003). In many cases, the transformed coefficients presented by some authors have been corrupted by errors and misprints (Kennett *et al.* 1978). Furthermore, when the point source and receiver are at comparable depths, integrands in the Green's functions oscillate with slowly decaying amplitude, demanding therefore the use of elaborated integration strategies (Hisada 1994; Kyum Kim *et al.* 2000). Although there are some scattering studies that properly consider the radiation condition in a layered half-space (e.g., Vogt *et al.* 1988; Luco *et al.* 1990; Grundmann *et al.* 1999; Kyum Kim *et al.* 2000; Kim *et al.* 2003), the intrinsic complexity of a multi-layer, dynamic fundamental solution certainly accounts for the reduced number of these studies, and its limited practical implementation.

This paper addresses the problem of finding a closed-form, two-dimensional (2D) SH Green's function for a layered half-space in the frequency-wave number domain suitable to be used in a discrete wave number boundary element (DWBEM) implementation (Kawase 1988). Contrary to other studies where the Green's function is nothing but a mathematical device, we rearrange our fundamental solution to be free from growing exponential terms, and customize it as the contribution of three terms, each one admitting a distinct physical interpretation: (1) an equivalent half-space; (2) source image impact; and (3) dispersive wave effect, respectively. Such an interpretation allows the proper use of analytical and numerical integration schemes. The correct treatment of Cauchy principal value integrals is also ensured. This, as a result, increases speed, results in greater accuracy, and sheds light on the conceptual aspects of the elastodynamic process. The scattering of 2D SH waves are the simplest problems in elastic wave propagation, since they can be studied independently from other body waves. The complexities added by the multiple layers on the other hand are so cumbersome that even under SH conditions, only numerical solutions are possible. In this work, we compute the multi-layered SH Green's function by using the stiffness matrix method (Kausel and Roësset 1981; Kausel 2006). As a first step, the proposed function is bounded to the condition in which the impulsive SH line source and the observation point are placed within the uppermost layer. Such a condition only has an impact over very deep scatterers within thin-layered media. Conversely, it does not have any restriction when examining surficial topography. We use the fundamental solution in the DWBEM scheme and test the benefits of our implementation by benchmarking our results against the solution of an infinitely long circular canyon subjected to oblique incident SH-plane waves within a homogeneous half-space. Our results show an excellent agreement with earlier reported solutions. Finally, we further shed light on the impact of layering by examining the dynamic response of a circular canyon within different configurations of horizontal strata and SH-incident angles.

2. *Frequency-Wave Number ($\omega - k$) Green's Function Formulation*

Figure 1 depicts the geometry of the layered system. The system is composed by N parallel layers ($N+1$ interfaces) in perfect welded condition, which ensures continuity of stresses and displacements throughout their sides. Layers are labeled sequentially. The first layer corresponds to the uppermost

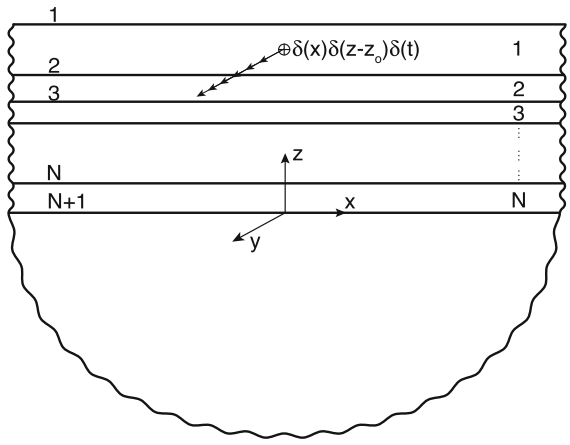

Figure 1
Layered half-space composed by N (N+1 interfaces) perfectly welded, parallel homogeneous layers. A unit impulsive SH line source acts at $x = 0$, $z = z_o$ in y direction within the uppermost superficial layer

superficial layer, while the Nth layer is immediately above the half-space. Each layer j is homogeneous with height, mass density, and shear modulus denoted by h_j, ρ_j, μ_j respectively. In the same direction, the half-space at the bottom can be considered as the N+1 layer with material properties $\rho_{\mathrm{hs}}, \mu_{\mathrm{hs}}$. No intrinsic damping is considered. This condition however, can be easily included by using the complex shear modulus $\mu_j^c = (1 + 2\mathrm{i}\xi_j)\mu_j$, where ξ_j is the material damping value for the layer j.

A unit impulsive SH line source acting in y direction is located at some elevation z_o within the first layer. The corresponding body force in the y direction is written as

$$b_y(x, z, t) = \delta(x)\delta(z - z_o)\delta(t). \tag{1}$$

Carrying out a double transform of Eq. (1), the body force representation in the $(\omega - k)$ domain yields

$$\tilde{b}_y(k, z, \omega) = \delta(z - z_o). \tag{2}$$

According to Kausel (2006), Eq. (2) is equivalent to a unitary traction distributed in a horizontal plane at $z = z_o$

$$p_y(k, z, \omega) = 1. \tag{3}$$

The $(\omega - k)$ stiffness matrix (Kausel and Roësset 1981; Kausel 2006) for a given layer j, and the half-space are denoted by $\mathbf{K}^j$, and K^{hs}, respectively. For SH waves, these matrices are written as

$$\mathbf{K}^j = \alpha_j\mu_j \begin{bmatrix} \coth(\alpha_j h_j) & -\mathrm{csch}(\alpha_j h_j) \\ -\mathrm{csch}(\alpha_j h_j) & \coth(\alpha_j h_j) \end{bmatrix};$$
$$K^{\mathrm{hs}} = \alpha_{\mathrm{hs}}\mu_{\mathrm{hs}}. \tag{4}$$

The stiffness matrix for the individual layer in compact form can be written as

$$\mathbf{K}^j = \begin{bmatrix} K_{11}^j & K_{12}^j \\ K_{21}^j & K_{22}^j \end{bmatrix}. \tag{5}$$

In Eq. (4), $\alpha_{(\bullet)} = \sqrt{k^2 - \frac{\omega^2}{\beta_{(\bullet)}^2}}\ \mathrm{Im}(\alpha) > 0$, is the vertical wave number, which depends on the shear velocity $\beta_{(\bullet)}$ of the jth layer (β_j), or half-space (β_{hs}) respectively.

The stiffness-matrix approach allows an interpretation in the same way as in structural analysis. Stiffness matrices for each individual layer are overlapped according to the contribution at each interface in order to obtain the impedance matrix for the entire system. In the same direction, the transformed SH line source from Eq. (3) is treated as an equivalent force applied throughout the top and bottom interfaces of the first layer. The relationship between interface forces and interface displacements is then

$$\begin{bmatrix} K_{11}^1 & K_{12}^1 & 0 & \cdots & 0 \\ K_{21}^1 & K_{22}^1 + K_{11}^2 & K_{12}^2 & \cdots & 0 \\ 0 & K_{21}^2 & K_{22}^2 + K_{11}^3 & \ddots & \vdots \\ \vdots & \vdots & \ddots & \ddots & \vdots \\ 0 & 0 & \cdots & K_{21}^N & K_{22}^N + K^{\mathrm{hs}} \end{bmatrix} \times \begin{bmatrix} \tilde{U}^1 \\ \tilde{U}^2 \\ U^3 \\ \vdots \\ \tilde{U}^N + 1 \end{bmatrix} = \begin{bmatrix} \tilde{F}^1 \\ \tilde{F}^2 \\ 0 \\ \vdots \\ 0 \end{bmatrix}. \tag{6}$$

The only non-zero values of the force vector in Eq. (6) are the first two entities. This is a direct consequence of having the impulsive SH line source acting only within the first stratum. Moreover, each sub-matrix and sub-vector are actually scalar functions of the wave number, frequency, and material properties instead of actual matrices or vectors. These two features allow some further simplification of the problem. Starting from the last equation, it is possible

to express the displacements of last interface $\tilde{U}^{N+1}$ in terms of those immediately above $\tilde{U}^{N}$. Replacing $\tilde{U}^{N+1}$ one more time in Eq. (6) , the system of equations is reduced by one unknown. Following the same strategy recursively, the matrix equation is greatly reduced into a system involving only the displacements and effective forces along the interfaces of the first layer. The explicit form of the matrix turns into

$$\alpha_1\mu_1\begin{bmatrix}\coth(\alpha_1 h_1) & -\mathrm{csch}(\alpha_1 h_1)\\ -\mathrm{csch}(\alpha_1 h_1) & \coth(\alpha_1 h_1)+\frac{\bar{K}^2_{\mathrm{hs}}}{\alpha_1\mu_1}\end{bmatrix}\begin{bmatrix}\tilde{U}^1\\ \tilde{U}^2\end{bmatrix} = \begin{bmatrix}\tilde{F}^1\\ \tilde{F}^2\end{bmatrix}, \tag{7}$$

where

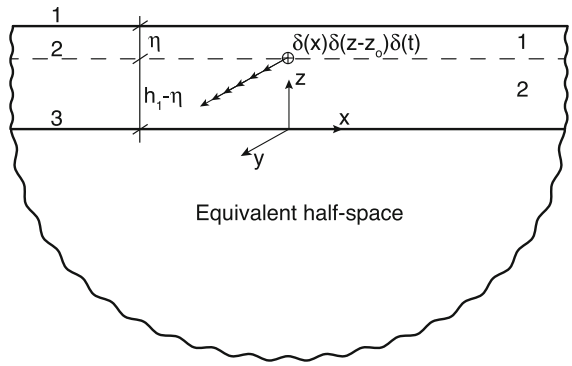

Figure 2
Single layer with auxiliary interface at the location of the impulsive source over an equivalent half-space. The auxiliary interface divides the layer into two layers of identical properties

$$\bar{K}^j_{\mathrm{hs}} = \begin{cases}\alpha_j\mu_j\left(\coth(\alpha_j h_j) - \frac{\alpha_j\mu_j}{\sinh^2(\alpha_j h_j)\left(\alpha_j\mu_j\coth(\alpha_j h_j)+\bar{K}^{j+1}_{hs}\right)}\right) & \text{for } j \le N\\ \alpha_{\mathrm{hs}}\mu_{\mathrm{hs}} & \text{for } j = N+1\end{cases}. \tag{8}$$

Of particular interest is the physical interpretation of the new reduced system. As can be readily seen, $\bar{K}^2_{\mathrm{hs}}$ represents the impedance of an equivalent half-space located at the second interface that, for fixed $(\omega - k)$ pairs, replaces all the underlying layers beneath the first stratum plus the original half-space.

The force vector in Eq. (7) corresponds to the equivalent forces exerted by the impulsive SH line source over the interfaces of the first layer. As in the finite element method, these forces are computed by using an appropriate set of shape functions in each layer. One way to circumvent the use of shape functions is by defining an artificial horizontal interface at the location of the impulsive source. The auxiliary interface divides the first layer into two layers, both having identical mechanical properties (Fig. 2.); as a result, the system in Eq. (7) is rearranged

$$\alpha_1\mu_1\begin{bmatrix}\coth(\alpha_1\eta) & -\mathrm{csch}(\alpha_1\eta) & 0\\ -\mathrm{csch}(\alpha_1\eta) & \coth(\alpha_1\eta)+\coth(\alpha_1(h_1-\eta)) & -\mathrm{csch}(\alpha_1(h_1-\eta))\\ 0 & -\mathrm{csch}(\alpha_1(h_1-\eta)) & \coth(\alpha_1(h_1-\eta))+\frac{\bar{K}^2_{\mathrm{hs}}}{\alpha_1\mu_1}\end{bmatrix}\begin{bmatrix}\tilde{U}^1\\ \tilde{U}^2\\ \tilde{U}^3\end{bmatrix} = \begin{bmatrix}0\\ 1\\ 0\end{bmatrix}. \tag{9}$$

The interface displacements are readily obtained by inverting Eq. (9). In fact, these displacements are already Green's displacements at the three corresponding interfaces. On the other hand, displacements at any other elevation z are computed by solving in both layers of Fig. 2. the double-transformed governing equation for SH wave propagation. Dirichlet conditions defined for the interface displacements from Eq. (9) apply. Because of space limitations, we will omit the mathematical procedure, and will only present the final expression for the frequency-wave number Green's function. In addition, the factor $e^{i(\omega t - kx)}$, where $i = \sqrt{-1}$, will also be

omitted, although it must be considered as present all the time.

$$\tilde{G}(k,z,z_o,\omega) = \frac{e^{-\alpha_1|z-z_o|}}{2\alpha_1\mu_1} + \frac{(1-\lambda)\left(e^{\alpha_1|z-z_o|}+e^{-\alpha_1|z-z_o|}\right)e^{-2\alpha_1 h_1}}{2\alpha_1\mu_1((\lambda-1)e^{-2\alpha_1 h_1}+\lambda+1)} + \frac{(1+\lambda)e^{-\alpha_1(2h_1-(z+z_o))}+(1-\lambda)e^{-\alpha_1(z+z_o)}}{2\alpha_1\mu_1((\lambda-1)e^{-2\alpha_1 h_1}+\lambda+1)}, \tag{10}$$

where $\lambda = \frac{\bar{K}_{hs}^2}{\alpha_1\mu_1}$, is the impedance ratio between the equivalent half-space and the first layer.

Equation (10) is the general solution for an impulsive SH line load acting within the top layer of a multi-layered medium. Clearly, in spite of the complicated nature of the problem, the general solution is remarkably simple. This in turn allows that some physical interpretations may be assigned to each term that comprises it. To begin with, the first term corresponds to the $(\omega - k)$ transform of an impulsive SH line source in a homogeneous unbounded space having mechanical properties as those of the top layer. This term controls the first stage of propagation when waves emanated from the line source are fully composed of cylindrical wave fronts. The cylindrical pattern is sustained up until any wave front reaches one of the two interfaces of the top layer. Furthermore, a closed-form inverse transform in the frequency–horizontal space coordinate domain $(\omega - x)$ is available in terms of Hankel functions (Achenbach 1973; Graff 1991); therefore, no discrete wave-number approach is needed for the full-space term in Eq. (10) . Regarding the second term of Eq. (10) , its implied cosine shape suggests that this term may control to some extent the influence of dispersive waves, as well as Love modes on the overall response. The dispersive nature is clearly seen by the dependence on λ. Finally, by looking at the power indices of the exponential function in the last term of Eq. (10) , it is possible to see that this term represents image point sources at elevations $z = 2h_1 - z_o$ and $z = -z_o$ respectively. These images, however, also exhibit dispersive features.

Along with the analytical verification of Eq. (10), the study of an impulsive anti-plane load applied at the interior of a homogeneous half-space is also of significant importance. As it is well-known, an explicit representation of the Green's function for a homogeneous half-space is available (e.g., Achenbach 1973; Graff 1991). Modeling a half-space as a layered one is readily achieved by giving the same mechanical properties to the whole arrangement of N parallel layers and the underlying half-space. Doing this renders $\lambda = 1$, which reduces Eq. (10) to

$$\tilde{G}_{\text{half-space}}(k,z,z_o,\omega) = \frac{e^{-\alpha_1|z-z_o|}}{2\alpha_1\mu_1} + \frac{e^{-\alpha_1(2h_1-(z+z_o))}}{2\alpha_1\mu_1}. \tag{11}$$

Equation (11) is precisely the exact solution in the $(\omega - k)$ domain for a homogeneous half-space (Achenbach 1973). Moreover, making $\lambda = 1$ rules out the second term in Eq. (10) , which is in full agreement with the fact that no propagation of Love waves is sustained for a homogeneous half-space, and consequently, endorses the physical interpretation previously given to this term.

Shifting the anti-plane line source horizontally to $x = x_o$, the layered Green's function

$$G(x,z,x_o,z_o,\omega) = \int_{-\infty}^{\infty} \tilde{G}(k,z,x_o,z_o,\omega)\exp^{-ikx}\,dk \tag{12}$$

is expressed as in Eq. (13), where $H_o^{(2)}(\cdot)$ is the second kind Hankel function of order zero. The variable Δ is the periodicity length of sources according to Bouchon and Aki (1977), while $r = \sqrt{(x-x_o)^2+(z-z_o)^2}$ denotes the distance between the impulsive source and the observation point. In short, Eq. (13) reads:

$$
\begin{aligned}
\mathrm{G}(x,z,x_o,z_o,\omega) = & \frac{-\mathrm{i}}{4\mu_1} H_o^{(2)}\left(\frac{\omega r}{\beta_1}\right) \\
& + \frac{1}{\Delta}\sum_{m=-Q}^{Q} \frac{(1-\lambda_m)\left(\mathrm{e}^{\alpha_{1_m}|z-z_o|} + \mathrm{e}^{-\alpha_{1_m}|z-z_o|}\right)\mathrm{e}^{-2\alpha_{1_m}h_1}}{2\alpha_{1_m}\mu_1((\lambda_m-1)\mathrm{e}^{-2\alpha_{1_m}h_1}+\lambda_m+1)} \mathrm{e}^{-\mathrm{i}k_m(x-x_o)} \\
& + \frac{1}{\Delta}\sum_{m=-Q}^{Q} \frac{(1+\lambda_m)\mathrm{e}^{-\alpha_{1_m}(2h_1-(z+z_o))} + (1-\lambda_m)\mathrm{e}^{-\alpha_{1_m}(z+z_o)}}{2\alpha_{1_m}\mu_1((\lambda_m-1)\mathrm{e}^{-2\alpha_{1_m}h_1}+\lambda_m+1)} \mathrm{e}^{-\mathrm{i}k_m(x-x_o)},
\end{aligned}
\tag{13}
$$

$$
\mathrm{G}(x,z,x_o,z_o,\omega) = \mathrm{G}_{\mathrm{Fs}} + \mathrm{G}_{\mathrm{Lw}} + \mathrm{G}_{\mathrm{Im}}, \tag{14}
$$

where $\mathrm{G_Fs}, \mathrm{G_L}w$, and $\mathrm{G_I}m$ represent the Green's functions associated to the full-space, Love waves, and point images respectively.

In order to avoid spurious contributions from adjacent sources, the length periodicity is chosen according to:

$$
\Delta \geq T_s \beta_{\max}, \tag{15}
$$

where T_s is the simulation time and $\beta_{\max}$ denotes the maximum shear velocity of the layered half-space. Furthermore, by using a complex frequency of the form $\tilde{\omega} = \omega - \mathrm{i}\omega_{\mathrm{I}}$ (Phinney 1965), accuracy is improved, while any additional fictitious contribution from adjacent sources is also removed (e.g., Bouchon and Aki 1977; Kawase 1988; Kawase and Aki 1989). In short, adding a constant imaginary part $\mathrm{i}\omega_{\mathrm{I}}$ to the angular frequency sampling $\Delta\omega$, shifts away poles of the Green's function from the real axis ω, which after traditional FFT synthesis renders an artificially damped domain response. The undamped response on T_s is retrieved later on after scaling the damped response by a factor $\exp^{\omega_{\mathrm{I}}t}$. Traditionally, the constant damped frequency ω_{I} only depends on T_s, and ranges between $\frac{\pi}{T_s} \leq \omega_{\mathrm{I}} \leq \frac{2\pi}{T_s}$ (Bouchon 2003). In our numerical simulations, we adopt the upper bound of this range, i.e., $\omega_{\mathrm{I}} = \frac{2\pi}{T_s}$. In Eq. (13), any discrete variable $(\cdot)_m$ is obtained after replacing $k_m = \frac{2\pi}{\Delta} m$ in its continuous definition.

3. Dynamic Response of a Cylindrical Canyon to Oblique Incident SH Waves: DWBEM Implementation

The scattering and diffraction of seismic waves by a canyon has received considerable attention since the initial work of Trifunac (1972). A complete list of the related studies is presented by Luco *et al.* (1990). Despite the simple geometry of the canyon, these studies exhibited very complicated interface patterns, as well as a strong space variation of the surface displacements. In the following, we present the integral equation representation of the boundary value problem, as well as the BEM discrete version that will be used later on in the verification stage.

3.1. Integral Representation of the Wave Motion

Consider a stack of N parallel layers laterally extending to infinity in the $\pm x$ direction. The uppermost interface is a free-traction surface. Every horizontal layer and the underlying half-space is homogeneous and exhibits different linear elastic mechanical properties. A region of smooth external surface S is removed from the first layer to form a canyon (Fig. 3). An oblique incident, anti-plane SH wave propagates inside the underlying half-space.

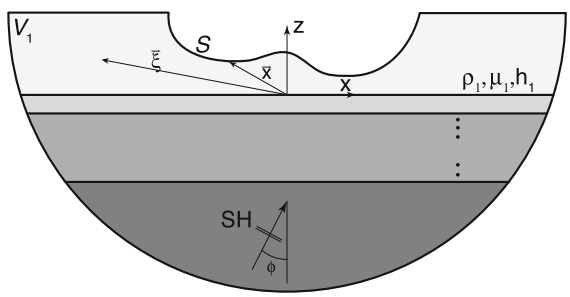

Figure 3
Layered half-space composed by N (N+1 interfaces) perfectly welded, parallel homogeneous layers. A region is extracted from the top layer to form a canyon of variable surface S. An oblique incident, anti-plane shear wave travels within the underlying half-space at an angle ϕ

The total motion at any material point $\mathbf{x} = (x, z)$ inside the region V_1 is expressed as the superposition of the free-field u^o plus the so-called scattered waves u^{sc}

$$u = u^o + u^{sc}; \tag{16}$$

in the same direction, the total traction field t^t is expressed as the contribution from the free-field and the scattered fields

$$t^t = t^o + t^{sc}. \tag{17}$$

Following the same ideas as in PAO and VARATHARAJULU (1976), the representation theorem (AKI and RICHARDS 2002) is used to express the scattered field in V_1 with implicit factor $e^{i\omega t}$ in terms of the total fields. In the absence of body forces, this relationship yields

$$u^{sc}(\boldsymbol{\xi}, \omega) + \int_S \mathrm{H}(\mathbf{x}, \boldsymbol{\xi}, \omega) u(\mathbf{x}, \omega)\, \mathrm{d}S = \int_S \mathrm{G}(\mathbf{x}, \boldsymbol{\xi}, \omega) t^t(\mathbf{x}, \omega)\, \mathrm{d}S, \tag{18}$$

where $\mathrm{G}(\mathbf{x}, \boldsymbol{\xi}, \omega)$ is the Green's function for a layered half-space given in Eq. (13). $\mathrm{H}(\mathbf{x}, \boldsymbol{\xi}, \omega)$ denotes the Green's traction function, i.e., the traction at point $\mathbf{x}$ on the surface S with specified normal vector $\mathbf{n}(\mathbf{x})$ due to a unit impulsive SH line source applied at point $\boldsymbol{\xi}$. For a linear elastic material under the assumption of small displacements, it is possible to express the Green's traction function in terms of the displacement Green's function Eq. (13) by applying the Hooke's law and the Cauchy's equation

$$\mathrm{H}(\mathbf{x}, \boldsymbol{\xi}, \omega) = \mu_1 \left(\frac{\partial \mathrm{G}}{\partial x} n_x + \frac{\partial \mathrm{G}}{\partial z} n_z \right). \tag{19}$$

Similar to Eq. (14), the simplified version of Eq. (19) is written as the superposition of traction Green's functions from the full-space, Love waves, and point images, respectively:

$$\mathrm{H}(\mathbf{x}, \boldsymbol{\xi}, \omega) = \mathrm{H}_{\mathrm{Fs}} + \mathrm{H}_{\mathrm{Lw}} + \mathrm{H}_{\mathrm{Im}}. \tag{20}$$

Because of the traction-free condition throughout S, the last term in Eq. (18) vanishes, and therefore, the integral representation of the scattered field reduces to

$$u^{sc}(\boldsymbol{\xi}, \omega) = -\int_S \mathrm{H}(\mathbf{x}, \boldsymbol{\xi}, \omega) u(\mathbf{x}, \omega) \mathrm{d}S. \tag{21}$$

The integral representation in terms of total displacements is readily obtained by replacing Eq. (21) into Eq. (16), as

$$u(\boldsymbol{\xi}, \omega) = u^o(\boldsymbol{\xi}, \omega) - \int_S \mathrm{H}(\mathbf{x}, \boldsymbol{\xi}, \omega) u(\mathbf{x}, \omega) \mathrm{d}S. \tag{22}$$

3.2. DWNBEM Formulation

The integral representation given in Eq. (22) needs to be transformed into an integral equation in order for us to be able to numerically solve it. This is accomplished by forcing $\boldsymbol{\xi}$ to lie in S.

$$c(\boldsymbol{\xi}, \omega) u(\boldsymbol{\xi}, \omega) + \int_S \mathrm{H}(\mathbf{x}, \boldsymbol{\xi}, \omega) u(\mathbf{x}, \omega) \mathrm{d}S = u^o(\boldsymbol{\xi}, \omega); \quad \boldsymbol{\xi} \in S. \tag{23}$$

In this case, the integrals in Eq. (22) exhibit singularities when $\boldsymbol{\xi} = \mathbf{x}$, which must be removed by a limiting process (DOMINGUEZ *et al.* 1993). This limiting process gives rise to the geometry-dependent factor $c(\boldsymbol{\xi}, \omega)$. A constant singularity contribution of $c(\boldsymbol{\xi}) = \frac{1}{2}$ is traditionally encountered when dealing with smooth surfaces and full-space Green's functions. In layered conditions on the other hand, additional terms in the Green's function such as the effect of point images preclude the idea of using a unique value.

To numerically solve Eq. (23), it is assumed that the boundary S is divided into K *constant-value* segments with a central node. This simple element, then, assumes that displacements and tractions are constant throughout each mesh element. When the collocation point is at the central node of element l, i.e., $\boldsymbol{\xi} = \mathbf{x}_l$, the discrete version of Eq. (23) is

$$c(l, \omega) u(l, \omega) + \sum_{k=1}^{K} \left[u(k, \omega) \int_{S_k} \mathrm{H}(\mathbf{x}_k, l, \omega) \mathrm{d}S_k \right] = u^o(l, \omega)$$
$$c(l, \omega) u(l, \omega) + \sum_{k=1}^{K} H(l, k) u(k, \omega) = u^o(l, \omega), \tag{24}$$

where $H(l, k) = \int_{S_k} \mathrm{H}(\mathbf{x}_k, l, \omega)\, \mathrm{d}S_k$ is the integral of the Green's traction function Eq. (17) over a generic

element k when the collocation point is at the l position. As for the term $c(l, \omega)$ the partition of Eq. (20) allows a straightforward evaluation of it. Since its first term is precisely the traction Green's function of a homogeneous, unbounded domain, its Cauchy principal value takes the well-known value of one-half. The contribution from the remaining terms is readily obtained either numerically or analytically. Indeed, as point sources locate away from the element, these do not exhibit any singularity when $\boldsymbol{\xi} = \mathbf{x}$. Moreover, since the last two terms in Eq. (20) are already expressed in the discrete wave number space, the singularities are already removed, and thus either traditional quadrature schemes or conventional analytic integrations are easily implemented.

$$c(l,\omega) = \frac{1}{2} + \int_{S_l} (\mathrm{H}_{\mathrm{Lw}}(\mathbf{x}_l, l, \omega) + \mathrm{H}_{\mathrm{Im}}(\mathbf{x}_l, l, \omega))\mathrm{d}S_l. \tag{25}$$

Because Eq. (19) is already a function based upon a discrete wave-number approach, Eq. (24) is the discrete wave number boundary element equation for the collocation point l.

Following the same procedure for every collocation point, a set of algebraic equations in terms of the unknown boundary values is established

$$\mathbf{H}_{(K,K)}\mathbf{u}_{(K,1)} = \mathbf{u^o}_{(K,1)}. \tag{26}$$

The unknown vector $\mathbf{u}_{(K,1)}$, is finally obtained by inverting Eq. (26).

3.3. Free-Field Computation

As is readily seen in Eq. (26), the unknown boundary values are the result of the free-field motions acting as point sources throughout the free boundary S. These free-field motions correspond to the response of the layered system in the absence of the canyon.

To compute the free-field response, it is convenient one more time to make use of the definitions shown in Fig. 1, and the stiffness matrix approach presented by Kausel (2006). As a first step, it is necessary to compute the free-field motions at each one of the N+1 interfaces. For doing this, it is required to compute the global stiffness matrix of the multi-layered system as in Eq. (6) . The stiffness matrices are, however, assembled for the horizontal wave number of the incoming wave

$$k = \frac{\omega}{\beta_{\mathrm{hs}}} \sin\phi. \tag{27}$$

In addition, one needs a re-formulated force vector expressed in terms of the incident wave at the N+1 interface Eq. (29) and the properties of the underlying half-space. The free-field displacements in each one of the N+1 interfaces is obtained then by inverting the next re-formulated set of algebraic equations

$$\left\{ \begin{bmatrix} K_{11}^1 & K_{12}^1 & 0 & \cdots & 0 \\ K_{21}^1 & K_{22}^1 + K_{11}^2 & K_{12}^2 & \cdots & 0 \\ 0 & K_{21}^2 & K_{22}^2 + K_{11}^3 & \ddots & \vdots \\ \vdots & \vdots & \ddots & \ddots & \vdots \\ 0 & 0 & \cdots & K_{21}^N & K_{22}^N + K^{\mathrm{hs}} \end{bmatrix} \begin{bmatrix} \tilde{U}^1 \\ \tilde{U}^2 \\ \tilde{U}^3 \\ \vdots \\ \tilde{U}^N + 1 \end{bmatrix} = \begin{bmatrix} 0 \\ 0 \\ 0 \\ \vdots \\ 2(\alpha_{\mathrm{hs}}\mu_{\mathrm{hs}})u^{\mathrm{inc}} \end{bmatrix} \right\}_{k=\left(\frac{\omega \sin\phi}{\beta_{\mathrm{hs}}}\right)} \tag{28}$$

$$u^{\mathrm{inc}}(x,0) = A\mathrm{e}^{\frac{\mathrm{i}\omega}{\beta_{\mathrm{hs}}}(h_t \cos\phi)}, \tag{29}$$

where A is the amplitude on the incident wave, h_t is the total sum of the layers depths, and ϕ is the incident angle.

The free-field displacements at the interior of the top layer at z elevations are finally obtained as

$$u^o(x,z,\omega) = \left[\frac{\sin(\alpha_1(h_1 - z))}{\sin(\alpha_1 h_1)}\tilde{U}^2 + \frac{\sin(\alpha_1 z)}{\sin(\alpha_1 h_1)}\tilde{U}^1\right] \times \mathrm{e}^{\mathrm{i}\left(\omega t - \frac{\omega \sin\phi}{\beta_{\mathrm{hs}}}x\right)}. \tag{30}$$

4. Verification

Results based upon the analytical Green's function Eq. (13) according to the DWBEM scheme shown in Eqs. (16) through (30) are tested with respect to widely verified results reported by

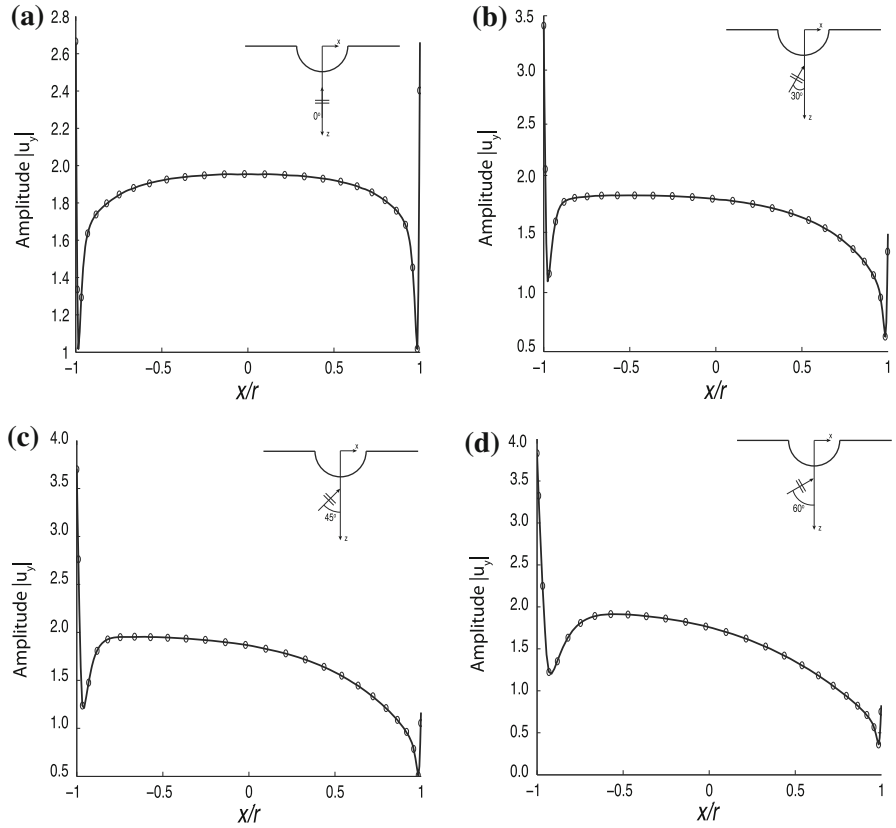

Figure 4
Surface displacement amplitudes $|u_y|$ versus x/r for a circular canyon within a homogeneous half-space. *Solid black lines* represent exact results according to TRIFUNAC (1972), hollow *black circles* represent the response from the DWNBEM with traction Green function as in Eq. (19). Four incident-angle scenarios are considered: **a** $\phi = 0^{\circ}$, **b** $\phi = 30^{\circ}$, **c** $\phi = 45^{\circ}$, **d** $\phi = 60^{\circ}$

TRIFUNAC (1972). Here, we consider a canyon of semi-circular cross section with radius $r = 1$ km in a homogeneous half-space with mechanical properties $\beta_{\text{hs}} = 1.0$ km/s and $\rho_{\text{hs}} = 1{,}000\,\text{kgm/m}^3$. As mentioned before, in order to obtain a half-space from a layered one, it only suffices to give the same properties to each stratum of the layered half-space. We consider four oblique incident SH-wave scenarios, i.e., $\phi = 0^{\circ}$, $\phi = 30^{\circ}$, $\phi = 45^{\circ}$, and $\phi = 60^{\circ}$, each one as a Ricker wavelet in time with $f_c = 1$ Hz ($f_{\text{max}} = 2.5$ Hz). The periodicity length chosen is $\Delta = 50$ km. Plugging in Δ and β_{hs} into Eq. (15) renders an available window time $T_s \leq 50$ s. All the simulations are, however, performed for a time window length of $T_s = 15$ s, which greatly avoids any fictitious contribution from adjacent sources. The complex frequency associated with this simulation time is $\omega_{\text{I}} = \frac{2\pi}{15}$ rad/s. To ensure the accurate propagation of the wave fields, the element length in DWBEM mesh is set to $\lambda_o/10$, where $\lambda_o = \beta_{\text{hs}}/f_{\text{max}}$ is the minimum wavelength expected. This criteria renders a mesh of 80 elements for modeling the circular canyon.

Figure 4 shows the maximum surface displacements amplitudes ($|u_y|$) versus x/r for four incident-wave scenarios. As is readily seen, the impact of the incident angle increases as its value grows. For vertical incident waves (Fig. 4a), the displacements are symmetrical, as expected. The maximum surface displacement amplitude is almost constant throughout the canyon surface with a value close to 2.0, as in the absence of the superficial irregularity. Under positive incident angles 4 (b), (c), and (d), the illuminated area shifts toward the left side of the canyon, increasing the surface amplitudes. Conversely, amplitudes over the shadow region (right side) decrease.

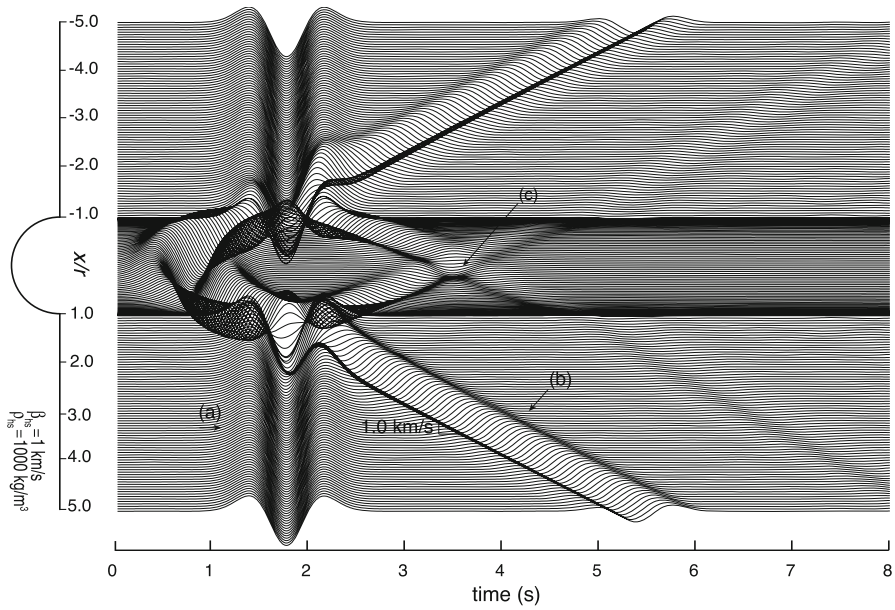

Figure 5
Synthetic traces at selected receivers throughout the free surface of a circular canyon within a homogeneous half-space. Seismic source is represented by a vertical-incident unit wave. A clear direct SH wave is observed at distances $|x/r| \geq 2$ (*arrow a*). Three diffracted SH waves are also present. The first two diffracted waves are induced by the *right* and *left* of corners the canyon (*arrow b*), while the late arrival (*arrow c*) is generated by the constructive interference of surface wave reverberations inside the canyon

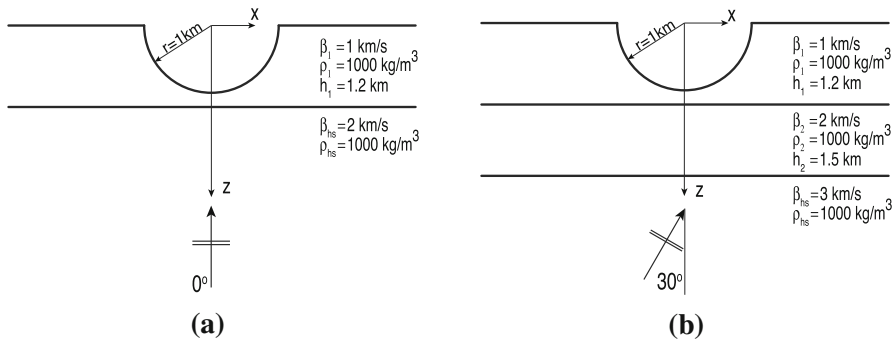

Figure 6
Semi-circular canyon within two different geotechnical settings: **a** One-layered half-space subjected to a vertical incident SH wave. **b** Two-layered half-space subjected to a 30° oblique incident SH wave

To further assess our results, we present synthetic traces for a vertical incident wave, i.e $\phi = 0^{\circ}$ at selected receivers along the free surface up to distances of $x/r = \pm 5$ (Fig. 5). Synthetic phases are obtained at any given point by solving Eq. (22). Because the only source of diffraction comes from the canyon geometry, all the surface wave fields are composed of SH waves. At the central region, no distinguishable Ricker pulse is possible because of strong diffraction effects from the canyon geometry during the entire dynamic response. On the other hand, at distances not so far away from the region of interest, i.e., $|x/r| \geq 2$, a direct Ricker pulse is clearly exhibited (arrow a). Two more noticeable phases are also present (arrows b, and c). The first diffracted SH phases (arrow b) are clearly induced by the left and

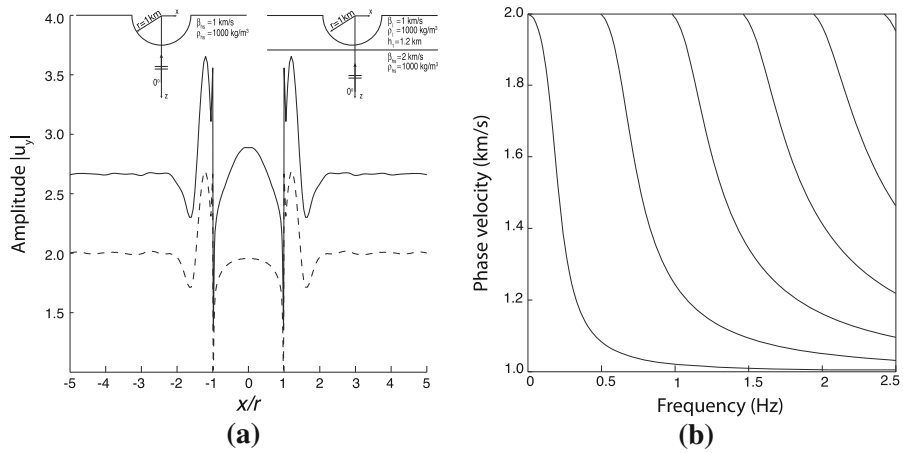

Figure 7

a Maximum surface amplitudes $|u_y|$ exhibited by an infinitely semi-circular canyon for a vertical-incident unit SH wave under two half-space scenarios. *Solid black line* represents the maximum surface response when a one-layered half-space (*top right*) is considered. *Dotted black line* represents the maximum surface amplitudes for a homogeneous half-space (*top left*). **b** Dispersion curves for a one-layered half-space. The *top layer* is characterized by $\beta_1 = 1$ km/s, $\rho_1 = 1{,}000$ kg/m^3, and $h_1 = 1.2$ km. The elastic parameters for the underlying half-space are $\beta_{hs} = 2$ km/s, and $\rho_{hs} = 1{,}000$ kg/m^3

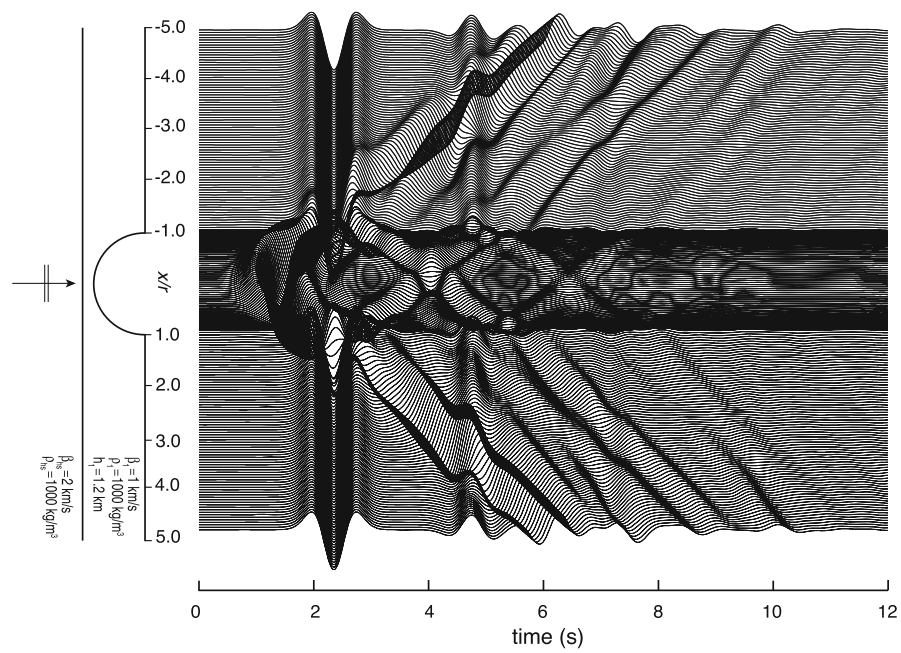

Figure 8

Synthetics of displacement at selected receivers throughout the canyon and the one-layered half-space free surface. The domain is subjected to a vertical-incident unit SH wave as a Ricker pulse in the time of 1 Hz central frequency

right corners of the canyon, while the last one (arrow c) is generated at the bottom of the canyon as a result of secondary reverberations of waves traveling along the circular cross section. Both phases, however, exhibit smaller surface amplitudes than those from the direct wave field. As was shown, our transparence tests present an unmistakable match when compared with exact results (Fig. 4), as well as exhibit a consistent spatial distribution of synthetic wave fields at distances far away from the region of

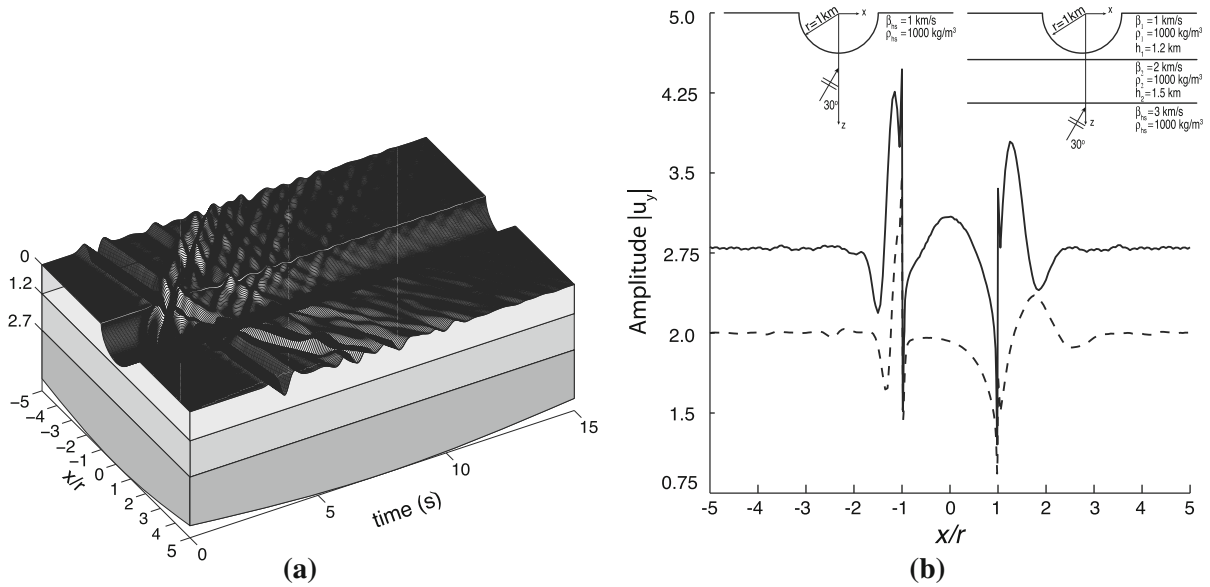

Figure 9

a Synthetics of displacement for a semi-circular canyon of $r = 1$ km within a two-layered half-space. The seismic source is a $\phi = 30^{\circ}$ incident Ricker pulse of $f_{\max} = 2.5 * \nabla\zeta$. **b** Maximum surface amplitudes throughout the canyon and free surface of the two-layered half-space scenario. Results are benchmarked against the homogeneous half-space solution

interest. This extreme accuracy is actually one of the consequences of dealing with an exact and explicit representation of the Green's function for the problem at hand.

5. *Numerical Results and Discussions*

We analyze the impact of one-, and two-layered half-spaces over the synthetics of displacement and spatial distribution of $|u_y|$ in a semi-circular cylindrical canyon of $r = 1$ km. The geotechnical setting for both examples is illustrated in Fig. 6. As in the verification stage $\Delta = 50$ km, $T_s = 15$ s, and $\omega_I = \frac{2\pi}{15}$ rad/s. We consider as seismic excitation a $\phi = 0^{\circ}$, and a $\phi = 30^{\circ}$ oblique incident, monochromatic SH wavelets as Ricker pulses of $f_{\max} = 2.5$ Hz. In both simulations, the circular canyon is modeled by 80 elements to properly accommodate the minimum wavelength expected.

Figure 7a depicts the spatial distribution of $|u_y|$ for the scenario illustrated in Fig. 6a. The spatial distribution is benchmarked against results from the homogeneous half-space condition. For $|x/r| \geq 1$, the maximum amplitudes $|u_y|$ follow a similar pattern in both simulations. Furthermore, maximum amplitudes for the layered condition can easily be found by scaling up the results from the homogeneous half-space by a factor of 1.35. On the other hand, at the interior region, i.e., $0 \leq |x/r| < 1$, results from the one-layered half-space exhibit the maximum amplification at the bottom of the canyon, as a consequence of geometric focusing (e.g., Tsaur and Chang 2009) and contrast impedance. The spatial distribution following a conic distribution contrasts to the circular-shaped envelope displayed by the homogeneous half-space.

Synthetics of displacement in the case of one-layered half-space are presented in Fig. 8. A clear first arrival is exhibited for $|x/r| > 2$ at $t = 2.2$ s. As in the homogeneous case, the corners of the canyon act as sources of diffracted waves, although high dispersion effects are notorious. Love waves resulting from seismic energy becoming trapped in the upper layer present lower amplitudes that the direct wave. This is explained partially by the fact that energy is split into one fundamental Love mode and at least four higher modes (Fig. 7b). Trapped Love waves, however, account for the larger duration of shaking.

Figure 9 presents the synthetics of displacement, and the spatial distribution of maximum amplitudes for the second example considered. Similar behavior to that shown in Fig. 8 is seen, although with strong

spatial variability, and significant effects of trapped Love waves. Displacement amplitudes take the maximum values at the corners of the canyon, which are more accentuated close to the left corner as consequence of the $\phi = 30^{\circ}$ incident angle. At distances $x/r < -1.0$, the spatial distribution of maxima under layered conditions is similar to those from the homogeneous case. Surprisingly, for $x/r > 1.0$, the layered spatial distribution appears as a mirror of the amplitudes under a homogeneous half-space scenario.

6. Conclusions

Following a stiffness matrix approach (Kausel and Roësset 1981), we presented a closed-form ($\omega - k$) Green's function in a multi-layered half-space for SH-wave propagation. It was shown that the proposed Green's function reduces exactly to the solution of the homogeneous half-space for $\lambda = 1$. Additionally, the multi-layered fundamental solution presents two salient features: (1) the original layered system can be reduced to a system composed by the uppermost superficial layer over an equivalent half space; and (2) the fundamental solution can be partitioned into three different functions, each one carrying out a different physical interpretation. Such a physical interpretation allows the proper use of analytical and numerical integrations, and the correct treatment of the Cauchy principal value integrals in BEM implementations. We implemented the fundamental solution in the DWBEM scheme to study the dynamic response of an infinitely long circular canyon to oblique incident SH waves under different layered half-space settings. Our results showed the significant impact that internal layering has over the spatial distribution of maxima, and the synthetics of displacement. In particular, internal layering has a tendency to lengthen the duration of shacking as consequence of trapped Love modes, as well as a significant displacement amplification due to impedance contrast effects in conjunction with geometric focusing.

Acknowledgements

The authors want to thank Universidad EAFIT (Medellín–Colombia) and COLCIENCIAS (the Colombian Institute of Science and Technology) for the institutional and financial support in this project. We also want to thank Juan Carlos Vergara Gallego for providing the results used for the validation.

References

Achenbach, J. (1973). Wave propagation in elastic solids, volume 16. North-Holland Amsterdam.

Aki, K. and Richards, P. (2002). Quantitative seismology. Univ Science Books.

Apsel, R. J. and Luco, J. E. (1983). *On the Green's functions for a layered half-space. Part II.* Bulletin of the Seismological Society of America, *73*(4):931–951.

Bouchon, M. (1981). *A simple method to calculate Green's functions for elastic layered media*. Bulletin of the Seismological Society of America, *71*(4):959–971.

Bouchon, M. (2003). *A review of the discrete wavenumber method*. Pure and Applied Geophysics, *160*(3–4):445–465.

Bouchon, M. and Aki, K. (1977). *Discrete wave-number representation of seismic-source wave fields*. Bulletin of the Seismological Society of America, *67*(2):259–277.

Chapman, C. (2003). *Yet another elastic plane-wave, layer-matrix algorithm*. Geophys J Int, *154*(1):212–223.

Chen, X. (1990). *Seismogram synthesis for multi-layered media with irregular interfaces by global generalized reflection/transmission matrices method. I. theory of two-dimensional SH case.* Bulletin of the Seismological Society of America, *80*(6A):1696–1724.

Chin, R., Hedstrom, G., and Thigpen, L. (1984). *Matrix methods in synthetic seismograms*. Geophys J Roy Astr S, *77*(2):483–502.

Dominguez, J. *et al*. (1993). Boundary elements in dynamics. Computational Mechanics Publications.

Dunkin, J. (1965). *Computation of modal solutions in layered, elastic media at high frequencies*. Bulletin of the Seismological Society of America, *55*(2):335–358.

Fuchs, K. and Müller, G. (1971). *Computation of synthetic seismograms with the reflectivity method and comparison with observations*. Geophys J Roy Astr S, *23*(4):417–433.

Gilbert, F. and Backus, G. (1966). *Propagation matrices in elastic wave and vibration problems*. Geophysics, *31*(2):326–332.

Graff, K. (1991). Wave motion in elastic solids. Dover publications.

Grundmann, H., Lieb, M., and Trommer, E. (1999). *The response of a layered half-space to traffic loads moving along its surface*. Archive of Applied Mechanics, *69*(1):55–67.

Haskell, N. (1953). *The dispersion of surface waves on multilayered media*. Bulletin of the Seismological Society of America, *43*(1):17–34.

Hisada, Y. (1994). *An efficient method for computing Green's functions for a layered half-space with sources and receivers at close depths*. Bulletin of the Seismological Society of America, *84*(5):1456–1472.

Hisada, Y. (1995). *An efficient method for computing Green's functions for a layered half-space with sources and receivers at close depths (part 2)*. Bulletin of the Seismological Society of America, *85*(4):1080–1093.

KAUSEL, E. (2006). Fundamental solutions in elastodynamics: a compendium. Cambridge University Press.

KAUSEL, E. and ROËSSET, J. M. (1981). *Stiffness matrices for layered soils*. Bulletin of the Seismological Society of America, *71*(6):1743–1761.

KAWASE, H. (1988). *Time-domain response of a semi-circular canyon for incident SV, P, and Rayleigh waves calculated by the discrete wavenumber boundary element method*. Bulletin of the Seismological Society of America, *78*(4):1415–1437.

KAWASE, H. and AKI, K. (1989). *A study on the response of a soft basin for incident S, P, and Rayleigh waves with special reference to the long duration observed in Mexico City*. Bulletin of the Seismological Society of America, *79*(5):1361–1382.

KENNETT, B. (1983). Seismic wave propagation in stratified media. Cambridge university press Cambridge.

KENNETT, B. and KERRY, N. (1979). *Seismic waves in a stratified half space*. Geophys J Roy Astr S, *57*(3):557–583.

KENNETT, B., KERRY, N., and WOODHOUSE, J. (1978). *Symmetries in the reflection and transmission of elastic waves*. Geophysical Journal of the Royal Astronomical Society, *52*(2):215–229.

KIM, M. K., LEE, J., and KIM, M. (2003). *Two-dimensional seismic response analysis of basin effects*. KSCE Journal of Civil Engineering, *7*(1):33–39.

KNOPOFF, L. (1964). *A matrix method for elastic wave problems*. Bulletin of the Seismological Society of America, *54*(1): 431–438.

KYUM KIM, M., MOOK LIM, Y., and WOO RHEE, J. (2000). *Dynamic analysis of layered half planes by coupled finite and boundary elements*. Engineering structures, *22*(6):670–680.

LUCO, J., WONG, H., and DE BARROS, F. (1990). *Three-dimensional response of a cylindrical canyon in a layered half-space*. Earthquake Eng. Struct. Dyn., *19*(6):799–817.

LUCO, J. E. and APSEL, R. J. (1983). *On the Green's functions for a layered half-space. Part I*. Bulletin of the Seismological Society of America, *73*(4):909–929.

PAO, Y. and VARATHARAJULU, V. (1976). *Huygens principle, radiation conditions, and integral formulas for the scattering of elastic waves*. The Journal of the Acoustical Society of America, *59*:1361.

PHINNEY, R. A. (1965). *Theoretical calculation of the spectrum of first arrivals in layered elastic mediums*. Journal of Geophysical Research, *70*(20):5107–5123.

SCHMIDT, H. and TANGO, G. (1986). *Efficient global matrix approach to the computation of synthetic seismograms*. Geophys J Roy Astr S, *84*(2):331–359.

THOMSON, W. (1950). *Transmission of elastic waves through a stratified solid medium*. J Appl Phys, *21*(2):89–93.

TRIFUNAC, M. D. (1972). *Scattering of plane sh waves by a semi-cylindrical canyon*. Earthquake Eng Struct Dyn, *1*(3):267–281.

TSAUR, D.-H. and CHANG, K.-H. (2009). *Scattering and focusing of SH waves by a convex circular-arc topography*. Geophysical Journal International, *177*(1):222–234.

VOGT, R., WOLF, J., and BACHMANN, H. (1988). *Wave scattering by a canyon of arbitrary shape in a layered half-space*. Earthquake Eng. Struct. Dyn., *16*(6):803–812.

WANG, L. and ROKHLIN, S. (2002). *Recursive stiffness matrix method for wave propagation in stratified media*. Bulletin of the Seismological Society of America, *92*(3):1129–1135.

WANG, R. (1999). *A simple orthonormalization method for stable and efficient computation of green's functions*. Bulletin of the Seismological Society of America, *89*(3):733–741.

(Received October 28, 2013, revised January 10, 2014, accepted January 17, 2014, Published online February 22, 2014)